

pubs.acs.org/Macromolecules Article

Poly(Isoprene)-Block-Poly(Ethylene Oxide) Diblock Copolymer Toughened Polylactide

Matthew C. Larson, Jonathan P. Coote, Frank S. Bates,* and Christopher J. Ellison*



Cite This: *Macromolecules* 2024, 57, 9334–9345



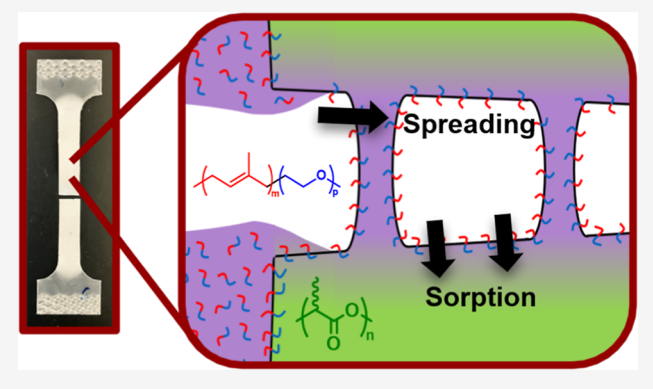
ACCESS

III Metrics & More

Article Recommendations

Supporting Information

ABSTRACT: Poly(lactide) (PLA) is currently the most successful bioderived synthetic polymer. However, applications of PLA are limited due to brittleness, which develops after about 1 day of physical aging at room temperature following melt processing. In this study, we investigate the ability of low molecular weight poly(isoprene)-block-poly(ethylene oxide) (IO) diblock copolymers to toughen glassy PLA. Melt blending IO with PLA leads to submicron diameter macrophase separated IO domains in the PLA matrix, stabilized by surfactant-like behavior associated with compatibility between the poly(ethylene oxide) (O) blocks and PLA. IO molecular weights that bracket the room temperature order-to-disorder transition temperature, $M_{\rm n}=1.7-3.3$ kg/mol, produce outstanding toughness with strains at break $\varepsilon_{\rm b}>150\%$, which persists



through 9 days of aging at room temperature. Higher molecular weight IO diblocks do not perform as well. We hypothesize that this behavior reflects two unique characteristics: (1) optimal particle sizes leading to cavitation and craze initiation when subjected to triaxial strain, and (2) draining of IO into the advancing crazes thereby stabilizing the porous craze structures. Experiments with melt mixed poly(isoprene) (I) homopolymer in PLA containing controlled particle sizes support this mechanism. These results demonstrate a general strategy for designing block copolymer additives that toughen otherwise brittle plastics.

1. INTRODUCTION

Synthetic plastics are a \$700 billion dollar industry which annually generates over 200 million metric tons (Mt) of plastic waste. PROUGHLY 70% of this waste is either landfilled or mismanaged, where it persists for decades to centuries. Holder a potential solution to this problem, since they can be broken down into less environmentally threatening products. Polylactide (PLA) is a commercial biosourced and industrially compostable alternative to oil-derived plastics with a global production of over 350,000 tons in 2022. Owing to a high elastic modulus and competitive tensile strength, PLA is the most commonly employed biopolymer in the agricultural, automotive, and packaging industries. However, PLA undergoes rapid physical aging and becomes brittle within hours of melt processing, limiting its potential applications.

One approach to addressing PLA's brittle behavior is by mechanical blending with rubber additives in the melt state, leading to micron size compliant domains which act as stress concentrators during deformation. ^{17,18} Rubber toughening of PLA has been extensively explored with additives such as poly(caprolactone), ^{19–22} polyethylene, ^{23,24} poly(butylene succinate), ^{25–27} and poloxamers. ²⁸ These blends often require substantial loadings of the additive (ca. > 10 wt %) to achieve adequate toughness, and can result in opaque materials which limits packaging applications. ^{29,30}

We previously demonstrated the benefits of blending Fortegra 100, a commercially available liquid poly(butylene oxide)-block-poly(ethylene oxide) (BO) diblock copolymer $[M_n = 7.4 \text{ kg/mol and containing } 38 \text{ wt } \% \text{ poly(ethylene)}]$ oxide)] with amorphous (PDLLA) and semicrystalline (PLLA) poly(lactide). 31-34 This additive forms micron-scale self-compatibilized domains in PLA, owing to the thermodynamic incompatibility of the poly(butylene oxide) (B) block with PLA and favorable interactions of the poly(ethylene oxide) (O) block with PLA. 35,36 Blends containing as little as 1.8 wt % BO in PLA showed up to a 20-fold increase in toughness and 26-fold increase in elongation at break.³¹ Through small-angle X-ray scattering, we showed that the BO domains cavitate and initiate crazes under uniaxial tension. 31,37 The toughness of these blends was attributed to multiple crazing as evidenced by uniform whitening at constant width of the gauge region during sample elongation.³¹ Additionally, BO

Received: July 31, 2024
Revised: September 9, 2024
Accepted: September 16, 2024
Published: September 26, 2024





is virtually refractive index matched with PLA resulting in remarkably transparent blends.³¹

Multiple crazing theory, first proposed in 1965 by Bucknall and Smith, accounts for the mechanical enhancement of many rubber toughened polymers, including various commercial products such as high-impact polystyrene (HIPS).³⁸⁻⁴⁰ This phenomenon is reported for glassy and semicrystalline polymers including polystyrene, polypropylene, and poly-(methyl methacrylate). 40-44 During bulk sample deformation, rubber particles first cavitate then initiate crazes from their equatorial axes, due to triaxial stress concentration in the polymer matrix.^{45–49} This results in the growth of many small crazes, enabling widespread matrix plastic deformation and energy absorption. 50,51 The rubber domains also can act as craze termination sites, preventing the growth of large isolated crazes which are likely to become cracks. 46,51 Maximum toughness through multiple crazing is reported to be favored by an optimal size distribution of rubbery inclusions: particles that are too small cannot cavitate and initiate crazes, whereas particles that are too large act as isolated macroscopic flaws leading to cracks and specimen failure. 42,48,52-55

Here we examine the toughening of glassy, amorphous PDLLA (herein referred to as PLA), using low molecular weight poly(isoprene)-block-poly(ethylene oxide) (IO) diblock copolymer additives, in order to further assess the deformation mechanism proposed to account for the previous results obtained with Fortegra 100. Blending 5 wt % IO (~38 wt % O and M_n between 1.7 and 11 kg/mol) with PLA leads to macroscopic phase separation due to thermodynamic incompatibility of poly(isoprene) (I) with the polyester. As with Fortegra 100, compatibility of the O block with PLA prevents phase coarsening through surfactant-like surface interactions with the matrix plastic and steric hindrance, leading to submicron diameter particles. 35,36,56-59 IO diblocks near the bulk order-disorder transition produced exceptionally tough blends, while higher molecular weight IO specimens generated marginal toughness. In addition, several low molecular weight I samples were blended with PLA and characterized mechanically.

The results of this experimental study are considered in the context of rubber cavitation and multiple crazing, along with a toughening mechanism proposed more than 3 decades ago by Argon, Cohen, and co-workers. They argued that draining of liquid additives from cavitated particles into associated crazes plasticizes craze growth and stabilizes the fibrillary craze morphology. $^{60-62}$ Our findings lend support for this mechanism and establish a general approach for the design of rubber additives to produce tough plastics.

2. MATERIALS AND METHODS

2.1. Materials. Amorphous PLA (4060D grade) was purchased from NatureWorks with an absolute number-average molecular weight $(M_{\rm n})$ of 96 kg/mol and dispersity (Đ) of 1.83, as determined by size exclusion chromatography (SEC) relative to PS standards (THF mobile phase, Mark—Houwink parameters K=0.0174 mL/g and $\alpha=0.736$ for PLA, and K=0.0128 mL/g and $\alpha=0.712$ for PS). ^{63,64} A series of IO diblock copolymers were synthesized via sequential anionic polymerization of I followed by O, according to previously reported protocols (Scheme S1). ⁶⁵ The I precursors to IO, end-capped with a hydroxyl group, were used as I homopolymers. Details regarding the synthesis and purification of IO diblock polymers are included in the Supporting Information. The numberaverage molecular weight of each block and mass fraction of poly(ethylene oxide) were determined by $^{\rm I}$ H NMR analysis as

shown in Figure S1. Mass fraction of O was converted to volume fraction, ($f_{\rm O}$, held constant at approximately 0.35), based on the densities of O ($\rho_{\rm O}=1.06~{\rm g/cm^3}$) and I ($\rho_{\rm I}=0.90~{\rm g/cm^3}$). Molecular weight dispersities (D) were determined by SEC with tetrahydrofuran (THF) as the mobile phase, and refractive index (RI) detection. Representative SEC traces are shown in Figure S2, molecular structures are shown in Scheme S2, and the characterization results for all the polymers are provided in Table 1, where the polymers are labeled to indicate the total molecular weight and identity (i.e., IO3 = poly(isoprene)-block-poly(ethylene oxide) of approximately 3 kg/mol).

Table 1. Characteristics of Synthesized Polymers

polymer	$M_{\rm n} ({\rm kg/mol})^a$	f_0^{b}	B^{c}	$T_{\text{ODT}}^{}}(^{\circ}\text{C})$
IO2	1.7	0.36	1.14	<20
IO3	3.3	0.36	1.10	85
IO6	5.6	0.35	1.09	190
IO7	7.1	0.34	1.09	235
IO11	10.8	0.36	1.08	300
I1	1.1	0	1.14	
16	6.4	0	1.07	

^aNumber average molecular weight was determined by end group analysis using ¹H NMR spectroscopy. ^bVolume fraction of O was calculated from relative ¹H NMR integrations using densities $\rho_{\rm I}=0.9$ g/cm³ and $\rho_{\rm O}=1.06$ g/cm^{3.63,64}. ^cDispersity was calculated from RI traces obtained by SEC with a THF mobile phase. ^dDetermined by DSC.

2.2. Methods. 2.2.1. Differential Scanning Calorimetry. (DSC) DSC analysis was performed using a Mettler Toledo DSC 1. Roughly 10 mg of sample was sealed in an aluminum pan, and calorimetry data was collected at heating or cooling rates of 10 °C/min under nitrogen. All samples were first heated from either 20 or 25 to 200 °C, cooled to -100 °C, then heated again to at least 200 °C. The glass transition temperature $(T_{\rm g})$ was taken from a second heating trace using midpoint half-height analysis in the Mettler-Toledo StarE software. The melting $(T_{\rm m})$ and crystallization $(T_{\rm c})$ temperatures are reported as the peak values of the associated endothermic or exothermic peak, respectively, and the order-to-disorder transition temperature $(T_{\rm ODT})$ is reported as the onset of a small exotherm according to previous methods. 68

2.2.2. Blending. Blends of PLA with ~5 wt % IO diblock copolymer or I homopolymer were prepared using a masterbatch dilution technique unless otherwise specified. A concentrated blend (called a masterbatch) was prepared by dissolving both IO or I and PLA pellets (12 wt % additive relative to PLA pellets) in 90 wt % chloroform. This solution was stirred for at least 8 h, then filtered and concentrated using a rotary evaporator. To fully remove the solvent, the masterbatch was manually cut into small pieces, then dried for 2 days at 65 °C and two additional days at 45 °C. Finally, the exact concentration of IO or I in the masterbatch was determined from an average of three ¹H NMR replicates.

Masterbatches were diluted to ~5 wt % additive using a recirculating 15 mL Xplore twin-screw microcompounder, with mixing performed for 5 min at 180 °C and 100 rpm under nitrogen. Neat PLA pellets were dried under vacuum for 24 h at 45 °C, and masterbatch pieces were used immediately after the second day of drying at 45 °C. Masterbatch pieces and PLA pellets were physically mixed, loaded into the microcompounder, blended, then extruded into cooling water. All blends were determined to be between 4.8 and 5.1 wt % IO or I in PLA by averaging two ¹H NMR replicates as shown in Figure S4. Neat PLA test specimens were processed by an identical solvent cast masterbatch and melt blend dilution technique. Absence of polymer degradation was confirmed by SEC in both neat PLA and a blend of PLA with IO2 (Figure S5).

2.2.3. Tensile Testing. PLA blends were compression molded into \sim 250 μ m thick films using a Carver hydraulic press operating at 135

°C and 2000 lbs compression. Pellets were pressed for 5 min unless otherwise specified, then rapidly quenched to room temperature within 1 min using a Wabash hydraulic press chilled with 15 °C cooling water. Dumbbell-shaped specimens were cut from these films according to ASTM D1708 using a dumbbell cutter (Dumbbell Co., Ltd. SDL200 equipped with an SDMK-1000 dumbbell cutter). Samples were aged for different periods of time on the benchtop prior to testing. A base case of two-days of aging was chosen as this produces brittle neat PLA samples; additional measurements were made after 9 days of aging. Finally, ten tensile tests were performed for each specimen on an Instron 5966 Universal Testing System operating at a 1 mm/min crosshead speed at room temperature to determine the Young's Modulus (E), the yield stress ($\sigma_{\rm y}$), the yield strain $(\varepsilon_{\rm v})$, the elongation at break $(\varepsilon_{\rm b})$, and the toughness. Details regarding the processing of tensile data are included in the Supporting Information

2.2.4. Small-Angle (SAXS) and Wide-Angle (WAXS) X-ray Scattering. SAXS/WAXS data were acquired from the 11-BM complex materials scattering (CMS) beamline at the National Synchrotron Light Source II (Brookhaven National Laboratory). Two-dimensional (2D) SAXS patterns were recorded using a Pilatus 2 M detector and sample-to-detector distance of 5.04 m, while WAXS patterns were collected using a Pilatus 800k detector and sample-to-detector distance of 0.403 m. All patterns were collected under vacuum with an incident beam energy of 17 keV (wavelength λ = 0.7294 Å) and calibrated with silver behenate. Neat IO samples were annealed at 135 °C, rapidly quenched, and aged at room temperature for 2 days to mimic film pressing prior to collecting scattering data. SAXS/WAXS traces were then recorded at 10 °C increments during heating. All IO/PLA blend scans were obtained at ambient temperature.

2.2.5. Transmission Electron Microscopy (TEM). Ultrathin TEM specimens (<100 nm thick slices) were cut from compression molded films using a diamond knife (Diatome) operated at -120 °C (Leica EM UC6 with FC-S Cryo attachment). Sections were exposed to the vapor from a 0.5 wt % ruthenium tetroxide (RuO₄) solution in water (Electron Microscopy Sciences) for 20 min which selectively stains I domains, ⁶⁹ then imaged using a TEM (Tecnai G2 Spirit Biotwin) at a 120 kV operating voltage. Images were processed and analyzed in FIJI software. Particle size distributions were determined based on image analysis of more than 1000 particles. If micelles were present, the percentage of micelles versus macrophase separated domains was estimated based on the relative areas of each in the image analysis (Figure S6).

2.2.6. Spreading Experiment. Analysis of a 5 μ L IO2 droplet spreading on a PLA surface was performed at 40 $^{\circ}$ C using a drop analyzer (Kruss DSA-30). The droplet diameter was monitored with time using ADVANCE software.

3. RESULTS AND DISCUSSION

3.1. Diblock Copolymer Thermal Properties and **Morphology.** DSC was employed to characterize crystallinity and microphase separation in the IO diblock copolymers. The T_{ODT} can be identified by DSC due to the small latent heat of this transition, which scales inversely with the magnitude of the segment–segment interaction parameter χ at the ODT. ^{68,70,71} ODT transitions are identified in the DSC traces shown in Figure 1 and the associated $T_{\rm ODT}$ values, ranging from 85 °C for IO3 to 300 °C for IO11 (i.e., inversely dependent on molecular weight) are listed in Table 1. No ODT was recorded for IO2, which remains disordered and liquid-like upon cooling to room temperature. All the IO diblock copolymers exhibit O crystallinity after cooling to -100 °C, evidenced by endotherms in the heating traces shown in Figure 1. Cooling at 10 °C/min from 100 °C leads to onset of crystallization by 20 °C except for IO2, which does not crystallize until -29 °C, with subsequent melting at 37 °C upon heating (see Figures S7-S9 and Table S1 for all crystallization and melting

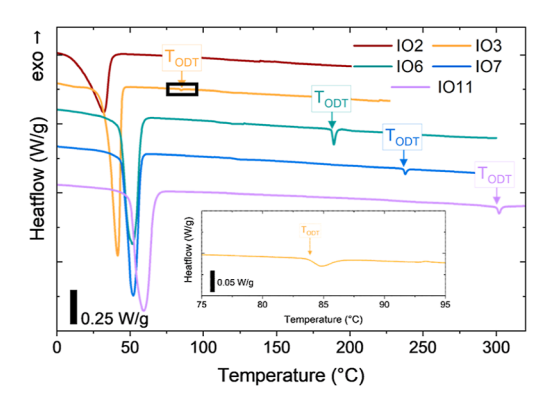


Figure 1. DSC thermograms during second heating cycle for neat IO copolymers. The inset magnifies the boxed region of the IO3 trace.

temperatures). These trends in crystallization and melting correlate with the expected behavior as a function of O block molecular weight.

The morphologies of the IO diblock copolymers were determined using SAXS. Selected SAXS traces for IO2, IO3, and IO7 are shown in Figure 2; a complete set of SAXS/ WAXS profiles are included in Figures S10-S14. SAXS data show evidence of O breakout crystallization in most IO samples, in which crystallization of the O block disrupts the microphase separated morphology formed during annealing at 135 $^{\circ}$ C. Heating above $T_{\rm m}$ leads to Bragg scattering consistent with hexagonally packed cylinders (HEX), except for IO2 which displays a single broad reflection associated with the disordered state at 40 °C (Figure 2A). Heating IO3 leads to disordering between 80 and 90 °C (Figure 2B) consistent with $T_{\text{ODT}} = 85 \,^{\circ}\text{C}$ as identified by DSC (Table 1). Overall, the IO diblock copolymer morphologies are consistent with the well-established phase behavior of semicrystalline diblock copolymers within the limits of soft confinement ($T_{\rm ODT} > T_{\rm c} >$ $T_{\rm g}$. 73-76

3.2. IO/PLA Blends. The morphology of the 5 wt % IO/ PLA blends following film pressing was investigated using a TEM. Figure 3 shows representative TEM micrographs of IO/ PLA blends, where the white spaces are holes created by the loss of IO particles during sample preparation. All the IO/PLA blends exhibit macrophase separation of IO, presumably due to the strong thermodynamic incompatibility of the majority poly(isoprene) blocks with PLA. S8,77 Magnified regions in Figure 3D,E reveal some micelle formation in blends containing IO7 and IO11, where dark circular domains of RuO₄ stained I blocks exhibit diameters of less than 10 nm. These micelles are anchored in the thin film sections through intercalation of the O blocks with PLA. Particle size distributions and estimated percent micellization are shown in Figure 4, with corresponding average diameters and variances based on log-normal fittings. The average particle size decreases with increasing IO molecular weight, varying from 690 nm for IO2 to 170 nm for IO11. We attribute this trend to a greater compatibilizing effect of the larger O chains at the IO/PLA interface as predicted by brush theory.⁷⁸ As shown in Figures S15-S18, different processing conditions, such as solvent casting versus melt blending, has little impact on the blend morphologies.

To characterize the internal morphology of the IO particles, SAXS data was acquired from two-day aged IO/PLA blends and compared to the neat IO SAXS patterns as shown in Figure 5. At ambient conditions, the IO/PLA blends show

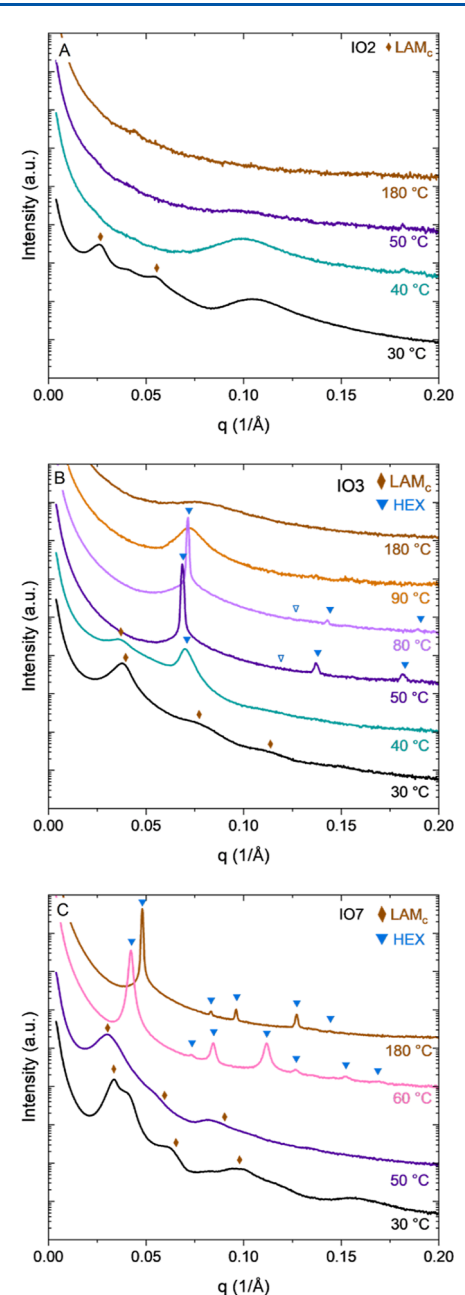


Figure 2. Representative 1D SAXS data for (A) IO2, (B) IO3, and (C) IO7 diblock polymer during heating cycles. Most specimens exhibit breakout crystallinity at 30 °C. Melting IO2 results in a disordered state while IO3 and IO7 transform to hexagonally packed cylinders (HEX), indexed by the blue triangles. Data shifted vertically for clarity.

clear evidence of microphase separation within the diblock copolymer particles, except for IO2 which appears to be disordered, but no evidence of crystallinity. Only a miniscule amount of O crystallinity was found in WAXS patterns for IO7 and IO11 blends, and none for the other blends as shown in Figure S19. Absence of strong higher order reflections (Figure S20) indicates a lack of long-range order, potentially due to the confinement of IO into submicron particle sizes documented in Figures 3 and 4.

The thermal properties of the melt molded and quenched IO/PLA films were further investigated using DSC following 2 days of physical aging. DSC thermograms from the first and

second heating cycles, shown in Figures 6 and S23, reveal a reduction in the T_g for PLA of approximately 5 °C (Table S2). This small reduction in T_g indicates partial mixing of O blocks with the PLA matrix; we do not expect this to alter the mechanical performance of the blends. 31,79,80 Except for the IO11 blend (and possibly the IO7 blend), there is no O crystallinity evident in the DSC traces in Figure 6, consistent with WAXS data (Figure S19), indicating that the blending process mostly suppresses O crystallization. Curiously, cooling the blends in the DSC to -100 °C prior to heating through $T_{\rm g}$ results in 19% to 41% O crystallinity as shown in Figure S21. We speculate that crystal nucleation is suppressed by the constraints associated with confinement of the IO phase within the hard glassy PLA matrix. Possible reasons include resistance to volume contraction that accompanies crystallization due to encasement of the particles within the glassy matrix (semicrystalline PEO has a density 11% greater than the amorphous state), 81 or constraints associated with the confined and curved phase boundaries. Regardless of the actual mechanism, the IO particles in the blends are either disordered and liquid-like (IO2), or microphase separated and rubbery (IO3, IO6, IO7,

3.3. Mechanical Properties of IO/PLA Blends. Uniaxial tensile tests were performed on IO/PLA blends after 2 and 9 days of aging at ambient conditions. Representative stress–strain data after 2 days of aging at room temperature are shown in Figure 7A, and the elongation at break $(\varepsilon_{\rm b})$ at both aging times is provided in Figure 7B; complete sets of stress–strain results are provided in Figures S22–S27 with a summary of all mechanical properties in Table S2. Neat PLA exhibits familiar brittle mechanical behavior after 2 days of aging, characterized by an elastic modulus E=3.0 GPa, and $\varepsilon_{\rm b}<10\%$. During sample elongation, neat PLA develops white streaks normal to the direction of deformation (shown in Figure S28), due to light scattered from voids formed during limited craze growth. 38,82

Blending PLA with the two lowest molecular weight IO diblocks, IO2 and IO3, results in 10 to 15-fold increases in toughness relative to neat PLA (Table S2). This behavior is characterized by average strains at break greater than 130% (Figure 7B), which are retained through 9 days of sample aging, similar to the previously reported behavior of Fortegra 100 blends. 31 There are modest reductions in sample modulus and yield strain, as well as a significant (~40%) reduction in the yield stress (Table S2). This reflects the capacity of IO particles to cavitate and initiate crazes at stresses lower than the intrinsic craze stress of pure PLA. ^{17,18,51} The reduction in yield stress is most significant for IO2, which is attributed to a larger average particle size.⁵² Figure 8A,B show that blends containing IO2 and IO3 exhibit uniform whitening during deformation starting at 10% elongation, without changes in sample width or thickness. This indicates that cavitation and crazing occur uniformly throughout the sample, which we attribute to the observed material toughness. Additional images depicting sample deformation are included in Figures S29-S30. Slight changes to the particle size of IO2 due to alternate blending protocols do not alter the mechanical performance (Figure S31).

Blend toughness declines as the IO molecular weight increases (Table S2 and Figure 7), where addition of 5 wt % IO11 results in no increase in strain at break relative to pure PLA (Table S2). Moreover, the mode of failure appears to change, where the IO7, IO11, and occasionally IO6 blends

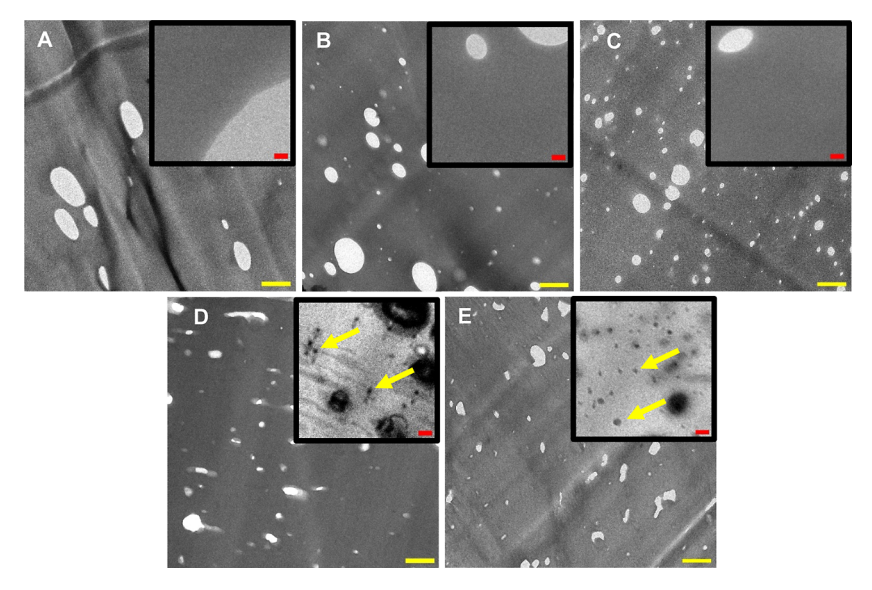


Figure 3. Representative TEM images of 5 wt % of (A) IO2, (B) IO3, (C) IO6, (D) IO7 and (E) IO11 blended with PLA. The yellow scale bar represents 1000 nm. The insets show magnified regions of each blend, where the red scale bar is 100 nm. The yellow arrows in (D) and (E) point to micelles in the IO7 and IO11 blends. No micelles were identified in blends with IO2, IO3, and IO6.

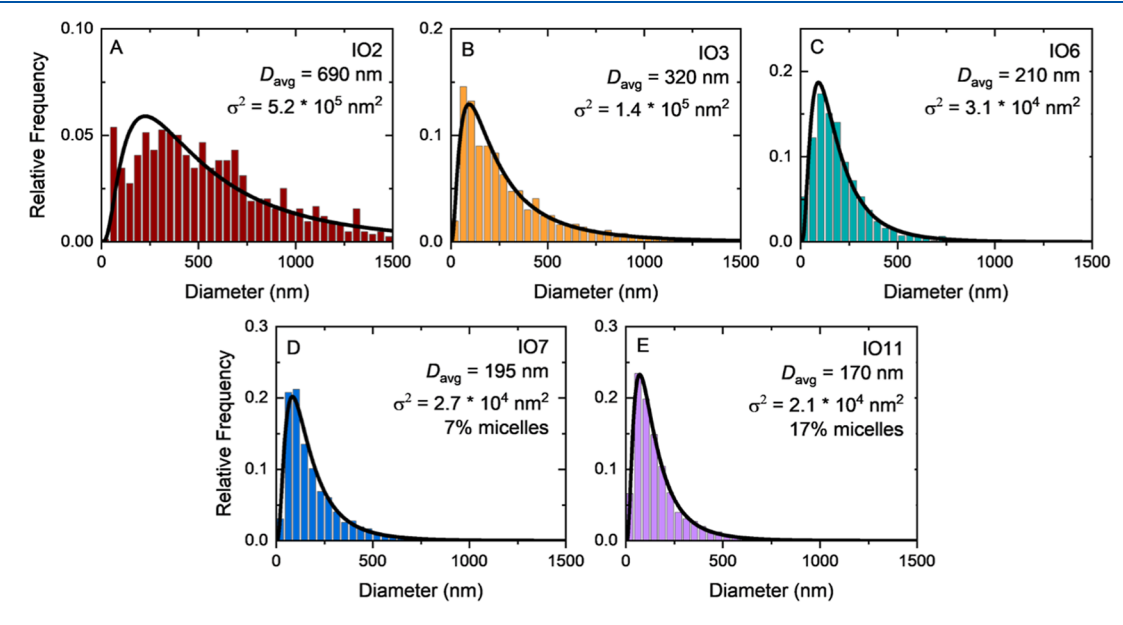


Figure 4. Particle size distributions of 5 wt % of (A) IO2, (B) IO3, (C) IO6, (D) IO7 and (E) IO11 diblock polymer blended with PLA. Average particle diameters (D_{avg}) and variances (σ^2) are based on log-normal fitting (solid black curves). Percent micelles was calculated using a relative area density of micelles to macrophase separated particles.

exhibit a tearing-like behavior during tensile deformation, as shown in Figure 8E. Visually, blends containing IO6, IO7, and IO11 exhibit stress whitening, consistent with cavitation and crazing. However, whitening appears to be inhomogeneous as shown in Figure 8 panels C-E, and Figures S32—S34, indicative of nonuniform crazing. As with IO2, modest changes to the particle size of IO11 due to processing variations do not alter the mechanical integrity of these blends (Figure S35).

3.4. Poly(Isoprene)/PLA Blend Morphology and Mechanical Performance. To isolate the role of the O blocks in the mechanical behavior of the IO/PLA blends, we prepared two poly(isoprene) homopolymers, I1 and I6 (Table 1), and devised mixing strategies with PLA that produced phase separated particle sizes that nearly span or exceed those found in Figure 4. Blend specimens were prepared with 5 wt %

I1 and I6 using the same procedure employed with the IO/PLA blends, which is referred to as I1a for the I1 additive. As shown in Figure 9A,B and quantified through image analysis in Figure 10A,B, these blends produced phase separated poly-(isoprene) particles with average diameters of 750 and 1600 nm, respectively. An alternative mixing protocol, called I1b, was performed as follows: solvent casting 5 wt % I1 with PLA from chloroform, drying under vacuum for 2 days at 65 °C followed by 2 days at 45 °C, then melt pressing at 135 °C for 45 s. This procedure resulted in a log–normal distribution of particle sizes with an average diameter of 400 nm (Figure 10C). The distribution of particles sizes in specimen I1a/PLA ($D_{\rm avg} = 750$ nm) and I1b/PLA ($D_{\rm avg} = 400$ nm) mimic the morphology of IO2/PLA ($D_{\rm avg} = 690$ nm) and IO3/PLA ($D_{\rm avg} = 320$ nm), respectively, while that of I6/PLA ($D_{\rm avg} = 1600$

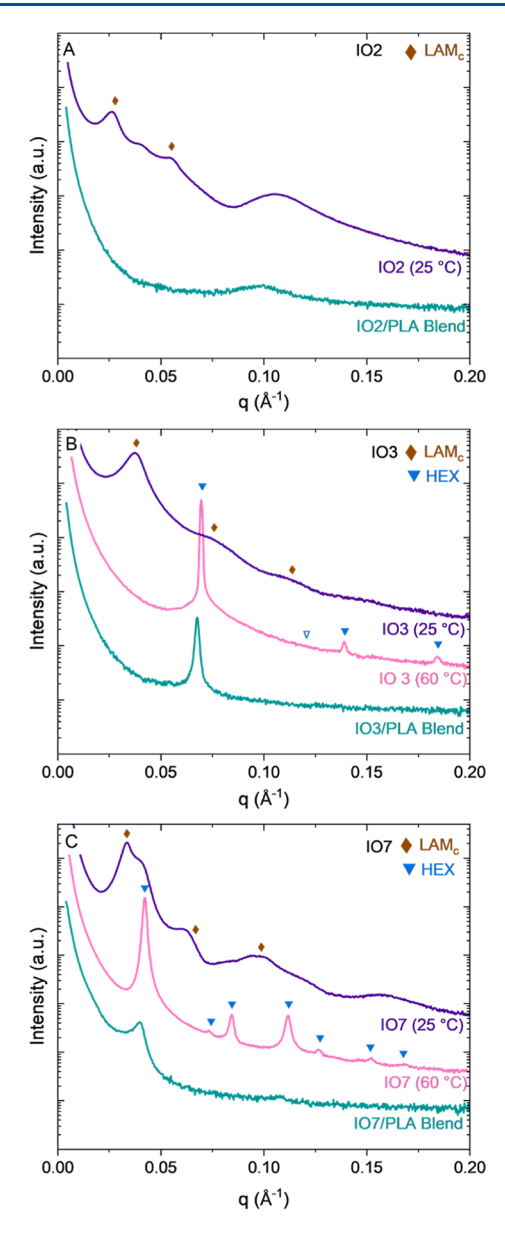


Figure 5. Representative SAXS data of neat IO diblock polymer at specified temperatures as well as 5 wt % blends of IO diblock with PLA for (A) IO2, (B) IO3 and (C) IO7. The purple data represents IO at ambient conditions, while the pink data shows IO at elevated temperature where a hexagonally packed cylinder morphology is observed. The teal data shows 5 wt % IO diblock polymer blended with PLA.

nm) far exceeds the distribution of particle sizes in IO2/PLA, which has the largest diameter diblock copolymer inclusions. DSC data for these blends (Figure S36, Table S2) demonstrate that the poly(isoprene) inclusions have no effect on the $T_{\rm g}$ of PLA due to incompatibility with this polyester.

Stress—strain data obtained from the I1/PLA blends after aging for 2 days is presented in Figure 11A, and the elongation at break is summarized in Figure 11B for 2 and 9 days of aging (full properties and all stress—strain curves are presented in Table S2 and Figures S37—S39). Blends containing I1 exhibit moderate toughness, but notably less than blends containing IO2 and IO3 despite similar particle size distributions. The I1 blends exhibit uniform stress whitening at 10% elongation as shown in Figures S40—S41, suggesting a homogeneous crazing

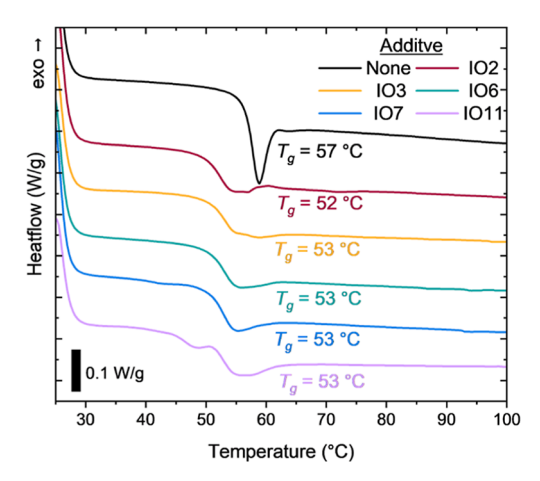
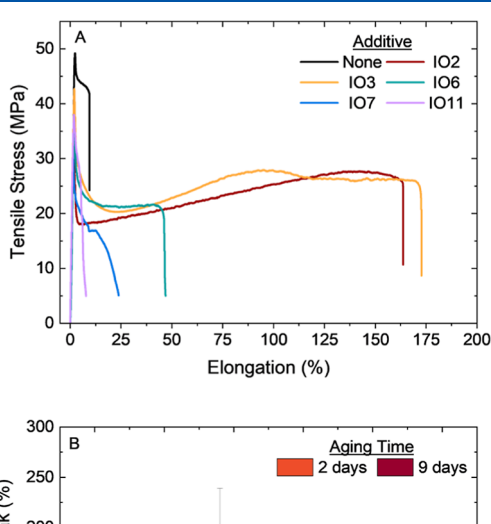


Figure 6. DSC thermograms during first heating cycle of 5 wt % IO additives blended with PLA. Samples were aged 2 days before testing.



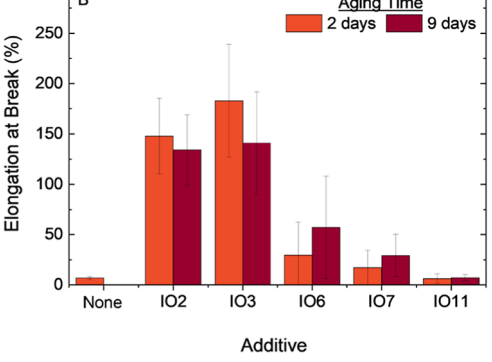


Figure 7. (A) Representative stress—strain data from PLA blended with 5 wt % of IO diblock copolymers after 2 days of aging under ambient conditions. (B) Elongation at break of PLA blended with 5 wt % IO averaged across 10 specimens. Error bars represent a standard deviation about the mean.

mechanism. Additionally, neither I1a/PLA nor I1b/PLA display necking or strain hardening behavior, which is observed in blends with IO2 and IO3 (Figure 7A). In comparison, the I6/PLA blend does not show uniform stress whitening, and instead displays patchy white streaks emerging normal to the direction of deformation, somewhat resemblant of IO6/PLA (Figures S42–S43). By 9 days of sample aging, the I6 blends are relatively brittle, with $\varepsilon_{\rm b}=21\pm11\%$, compared to 82 \pm 22% for I1a/PLA, and significantly inferior to IO2/PLA and IO3/PLA.

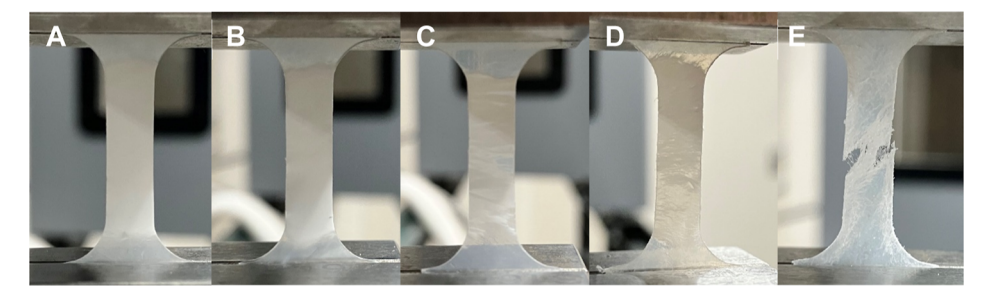


Figure 8. Representative gauge regions at 10% elongation of (A) IO2, (B) IO4, (C) IO6, (D) IO7, and (E) IO11 blended with PLA. All samples were aged at ambient conditions for 2 days prior to tensile testing.

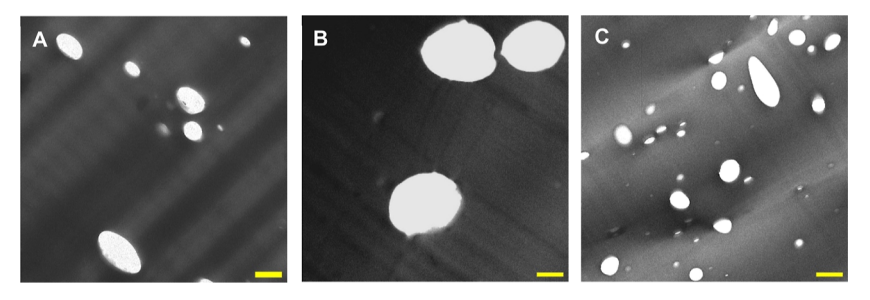


Figure 9. Representative TEM images of 5 wt % of (A) I1a, (B) I6, and (C) I1b blended with PLA. The yellow scale bar represents 1000 nm.

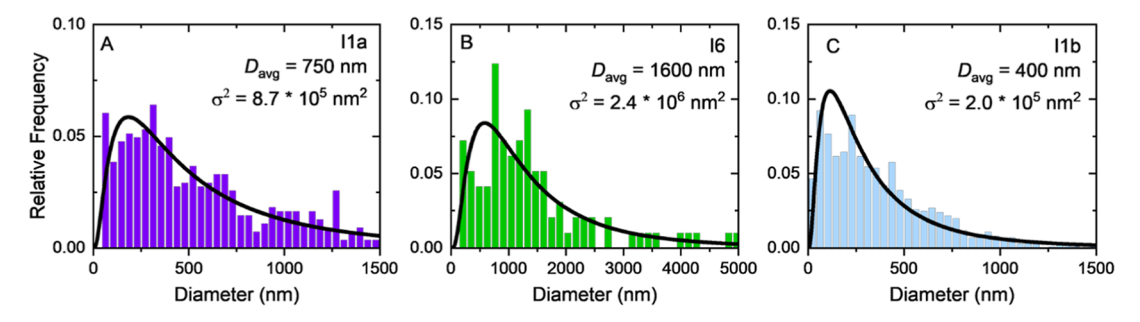


Figure 10. Particle size distributions of 5 wt % of (A) I1a with a short molding time, (B) I6, and (C) I1b blended with PLA. Average particle diameters (D_{avg}) and variances (σ^2) are based on log–normal fitting (solid black curves).

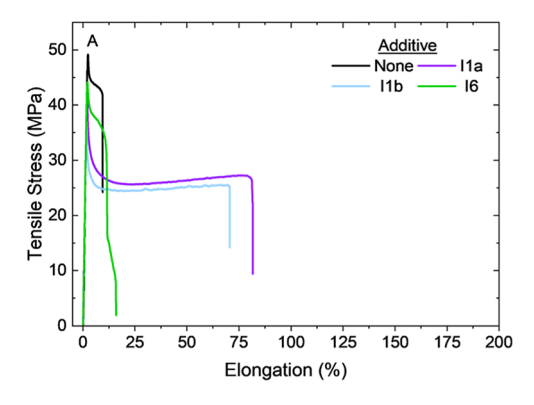
3.5. Toughening Mechanism. The size of rubbery inclusions represents a critical factor in toughening plastics by multiple crazing, where there are both upper and lower bounds to the range of effective particle sizes. 48,49,52,54 The limits on particle size are generally accepted to be between 500 and 1100 nm for PLA. 31,53,83,84 On the low end, particles must be large enough to concentrate a critical stress over a critical distance resulting in cavitation and craze initiation. 39,85 We employ a model for particle cavitation developed by Bucknall and Paul 48,49 in which the energy change associated with particle cavitation (ΔU) is given by

$$\Delta U = \frac{2}{3} \pi R_{\rm p}^{3} K^{*} \left(\varepsilon_{\rm rV0} - \frac{r_{\rm v}^{3}}{R_{\rm p}^{3}} \right)^{2} + 4\pi r_{\rm v}^{2} \Gamma$$
$$- \frac{2}{3} \pi R_{\rm p}^{3} K^{*} \varepsilon_{\rm rv0}^{2}$$
(1)

where $R_{\rm p}$ is the particle radius, $r_{\rm v}$ is the radius of the void formed during cavitation, Γ is the rubber-void surface energy, and K^* and $\varepsilon_{\rm rV0}$ are the effective modulus and initial volume strain of a hypothetical rubber particle accounting for both particle and matrix effects, respectively. ΔU accounts for energy release of both the particle and matrix during cavitation, which becomes favorable when $\Delta U < 0$ (i.e., cavitation enables

the material to absorb energy). A plot of ΔU for various rubber particle sizes is shown in Figure 12, based on $\Gamma = 35 \text{ mJ/m}^2$, $K^* = 0.95$ GPa, and $\varepsilon_{rV0} = 1.1\%$ (see details in Supporting Information). Simultaneously solving $\Delta U = 0$ and $\partial \Delta U / \partial r = 0$, leads to an estimated critical particle size for cavitation of D =150 nm. This relatively crude calculation suggests that a lower bound on particle size for cavitation may exist near the average particle diameters of IO7/PLA and IO11/PLA leading to the brittle behavior of these blends. The stiff nature of IO7 and IO11 particles caused by strong microphase separation likely presents further barriers to particle cavitation. Additionally, the observed tearing behavior in blends with IO6, IO7, and IO11 resembles behavior reported for blends of PLA or PS containing rigid fillers, in which tearing is attributed to debonding at the particle/matrix interface due to an inability of the particles to cavitate.86-88

While a small particle size restricts cavitation and craze initiation, a large particle size also presents barriers to craze toughening. Such results have been reported in blends of PLA with poly(caprolactone), and blends of polystyrene (PS) with poly(butadiene).^{53–55} This likely explains the mechanical performance of the I6/PLA blend, which shows only minimal improvements in mechanical integrity after 9 days of sample aging. Notably, this blend has an average particle diameter of



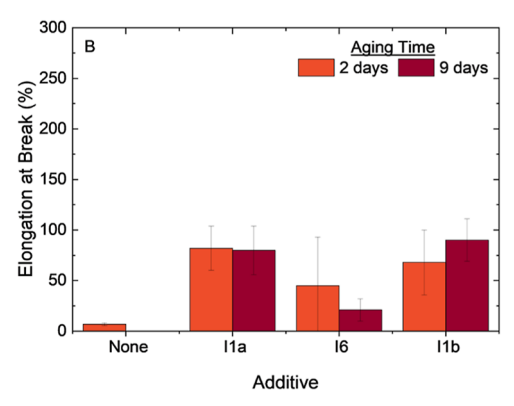


Figure 11. (A) Representative stress—strain data of PLA blended with 5 wt % of I additives after 2 days of aging under ambient conditions. (B) Elongation at break of PLA blended with 5 wt % I additives averaged across 10 specimens. Error bars represent a standard deviation about the mean.

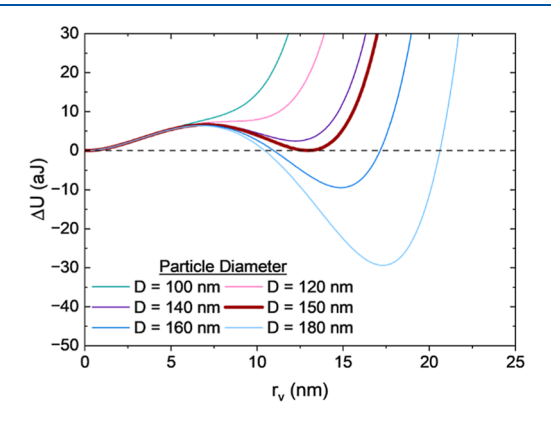


Figure 12. Energy change ΔU after cavitation as a function of IO particle size in PLA matrix at 5 wt % rubber.

1600 nm, more than twice that of any other additive. As shown in Figure 9C, this results in fewer particles per unit volume, and accordingly fewer crazes initiated under tension. Furthermore, crazes that do form are less likely to intersect existing I6 particles, resulting in the formation of a few large crazes, which are more likely to become cracks and result in sample failure. Heffer, large particle sizes result in insufficient craze initiation and termination, and ultimately brittle blend behavior.

We believe that the IO2, IO3, and I₁ blends with PLA have particle sizes within the optimal window for craze toughening. All four blends are tough, independent of aging up to 9 days, and show uniform sample whitening indicative of homoge-

neous, multiple craze formation. The mechanical performance of both I1a/PLA and I1b/PLA is consistent with previous reports of multiple crazing, with similar changes in tensile toughness and elongation at break (i.e., 10-fold increase in $\varepsilon_{\rm b}$). The mechanical performance of both I1 blends is nearly identical, suggesting that both particle sizes lie in the optimal window for cavitation initiated crazing.

As previously argued by Argon, Cohen, and co-workers, highly mobile polymer chains within craze-initiating particles may influence toughening efficacy. $^{60-62,89}$ They hypothesized that in blends of PS with a minority of PB, the liquid-like homopolymer comprising PB particles could drain along a growing craze surface, then sorb into and plasticize the craze/ matrix interface and fibrils, which facilitates craze growth. 60-62,89 This draining behavior may occur in the I1a/ PLA and I1b/PLA blends. However, we believe the IO diblock copolymers, like Fortegra 100, have several advantages that amplify this mechanism. First, the I block is strongly incompatible with PLA, which promotes particle formation and prevents the entire diblock from solubilizing with PLA during deformation and spreading, like the behavior of PB blended with PS as reported by Argon, Cohen et al. 60-62,89 Second, owing to the negative interaction parameter between PEO and PLA (χ < 0), the O block enables localized sorption and plasticization at the craze/matrix interface, further facilitating craze growth. ^{35,36} Finally, the surfactant-like nature of IO in contact with the PLA melt enables particle size refinement and suppression of domain coarsening during processing due to steric stabilization. We hypothesize that this spreading and sorption behavior, as depicted schematically in Figure 13, allows crazes to propagate at lower applied stresses, and prevents premature craze fracture.

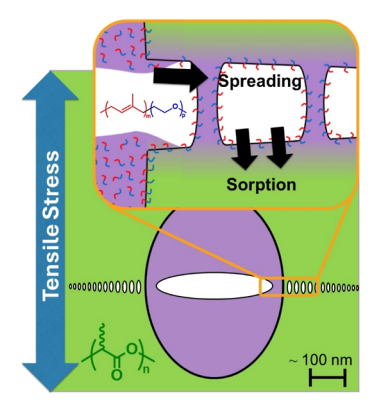


Figure 13. Proposed mechanism of spreading and sorption for IO in PLA during tensile deformation.

The spreading velocity of IO2 was estimated from the rate at which a 5 μ L IO2 droplet expands on a neat PLA film. This experiment was performed at 40 °C to overcome limitations of neat IO2 crystallinity ($T_{\rm m}=37$ °C), noting that IO2 is a disordered liquid at $T>T_{\rm m}$ and in PLA blends. After the initial rapid change in radius due to gravity, associated with the first 2 min of the experiment, the change in droplet radius with time was used to estimate a velocity of IO2 propagation on a PLA surface of 0.93 μ m/sec, as shown in Figure 14. It is likely that this value is a lower bound on the spreading rate of IO2 within a growing craze, given the small geometry of a craze tip (<20 nm) in which capillary forces would be expected to increase the spreading rate. ^{37,90} The velocity at which a PLA craze tip

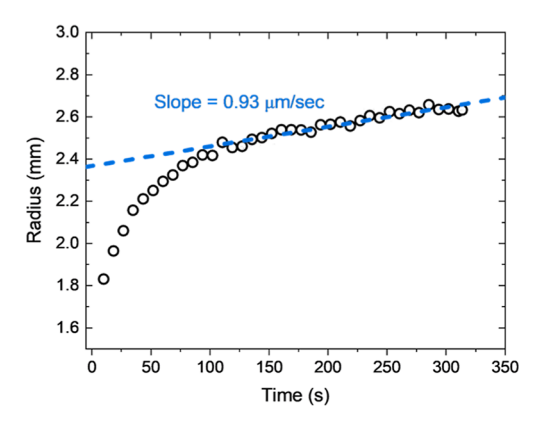


Figure 14. Radius of a 5 μ L drop of IO2 on PLA at 40 $^{\circ}$ C measured at various time points.

advances through the plastic has not been reported, but steady-state craze tip velocities for other plastics range between 0.01 and 1 μ m/sec, 91-94 implying that IO2 should be able to wet a growing craze surface at a rate greater than or equal to the rate at which new craze surface is formed.

Differences in the mechanical performance of the I1/PLA and IO/PLA blends further support a craze growth plasticization phenomenon. First, the IO/PLA blends exhibit strain hardening and necking. We hypothesize this is due to IO sorption at the craze/matrix interface, which enables a plasticized craze growth process and greater chain alignment within the craze microstructure. In comparison, the incompatibility of I with PLA prevents sorption at the craze/matrix interface, resulting in sample elongation at constant stress as commonly reported for multiple crazing. 37,81-83 Further, IO2 has a higher necking strain (134 \pm 9%) than IO3 (84 \pm 13%), indicative of more extensive craze growth in IO2 blends. This may be attributed to the greater mobility of IO2 given it is in a disordered state. Higher mobility facilitates spreading through propagating crazes, enabling greater overall craze growth prior to the onset of cold drawing. Finally, the flow stress, taken as the minimum in tensile stress following sample yielding, is higher for I1/PLA blends (26 \pm 1 MPa for I1a/PLA, 24 \pm 1 MPa for I1b/PLA) than for IO2 (18 \pm 1 MPa) or IO3 (21 \pm 1 MPa). This again offers support of plasticized fibril drawing, and that the IO additive sorbs into the craze growth region to enable craze propagation at lower stress.

It is puzzling that microphase separated IO3 is as effective in toughening PLA as the disordered and liquid-like IO2. Our postulated toughening mechanism relies on cavitation, spreading, and wetting of craze surfaces by the IO diblock copolymer. In the microphase separated state, with $T_{\rm ODT}$ = 85 °C, IO3 is a soft solid that will not flow like a liquid. The relatively sharp peak in the SAXS profile for the IO3/PLA blend (Figure 5B) indicates that such a structure exists within the $D_{avg} = 320$ nm diameter particles. We speculate that this state of intermediate segregation is disrupted by the triaxial stress and cavitation of the IO3 particles, leading to disorder and flow. This hypothesis is consistent with SAXS data obtained from the IO3/PLA during elongation, which shows that reduction in and eventual elimination of the sharp peak associated with the microphase separated state in the undeformed blend (Figure S44). These results suggest that microphase separation in the IO3 particles is destroyed during sample elongation, which would enable the proposed spreading and craze plasticization behavior. Alternatively, IO3 can be crystallized in situ (as shown in Figure

S45) by soaking an IO3/PLA film in liquid nitrogen for 10 min, resulting in 30% PEO crystallinity when heated to room temperature. However, crystallizing IO3 does not result in a loss of sample toughness (Figures S46 and S47). In fact, DSC first heating scans taken both before and after tensile testing suggest the crystals are mechanically melted during tensile deformation (Figure S48).

4. CONCLUSIONS

This investigation establishes a general approach to toughening brittle plastics with block copolymers, motivated by a prior discovery that the commercial diblock copolymer marketed under the trade name Fortegra 100 when blended with PLA leads to remarkable toughness even after months of aging. Here, a set of poly(isoprene)-block-poly(ethylene oxide) (IO) diblock copolymers are shown to exhibit the same behavior at molecular weights that place the pure diblock material just below and just above a room temperature order-disorder transition temperature, T_{ODT} . Blends with glassy PLA containing 5 wt % of these optimized compounds exhibit strains at break $\varepsilon_{\rm b}$ > 150% after 9 days of aging at room temperature following melt molding of specimens. Pure PLA fails at $\varepsilon_{\rm b}$ < 10% after 2 days of aging. Higher molecular weight IO, characterized by $T_{\rm ODT} \geq 190$ °C, failed to impart tensile toughness when blended with PLA. This remarkable behavior is attributed to two factors: (1) stable average IO particle sizes conducive to cavitation under triaxial strain leading to craze initiation, and (2) draining of the IO block copolymer into the advancing crazes resulting in stabilization of the porous craze structures. Additional experiments with melt blended I homopolymer support this two-step mechanism. These findings should be generally applicable to toughening of brittle plastics.

ASSOCIATED CONTENT

Supporting Information

The Supporting Information is available free of charge at https://pubs.acs.org/doi/10.1021/acs.macromol.4c01832.

Polymer synthesis and characterization information, methodology considerations, DSC data regarding the crystallinity of IO copolymers, SAXS/WAXS data for all IO copolymers, TEM micrographs, particle size distributions, and mechanical data of alternate IO2/IO11 blending procedures, additional scattering and DSC data of IO/PLA and I/PLA blends, stress—strain data and visual representations of deformation in IO/PLA blends, details regarding particle cavitation criterion, in situ tensile SAXS of IO3/PLA blends, and in situ crystallization data (DSC and stress—strain data) of IO3/PLA blends (PDF)

AUTHOR INFORMATION

Corresponding Authors

Frank S. Bates — Department of Chemical Engineering and Materials Science, University of Minnesota, Minneapolis, Minnesota 55455, United States; orcid.org/0000-0003-3977-1278; Email: bates001@umn.edu

Christopher J. Ellison — Department of Chemical Engineering and Materials Science, University of Minnesota, Minneapolis, Minnesota 55455, United States; orcid.org/0000-0002-0393-2941; Email: cellison@umn.edu

Authors

Matthew C. Larson — Department of Chemical Engineering and Materials Science, University of Minnesota, Minneapolis, Minnesota 55455, United States; orcid.org/0000-0002-6445-0882

Jonathan P. Coote — Department of Chemical Engineering and Materials Science, University of Minnesota, Minneapolis, Minnesota 55455, United States; orcid.org/0000-0002-2727-4840

Complete contact information is available at: https://pubs.acs.org/10.1021/acs.macromol.4c01832

Notes

The authors declare no competing financial interest.

ACKNOWLEDGMENTS

This work was supported primarily by the farm families of Minnesota and their corn check-off investment and in part by the National Science Foundation Center for Sustainable Polymers at the University of Minnesota, a Center for Chemical Innovation (CHE-1901635). Parts of this work were carried out in the Characterization Facility, University of Minnesota, which receives partial support from the NSF through the MRSEC (Award Number DMR-2011401) and the NNCI (Award Number ECCS-2025124) programs. Part of this work also used the 11-BM Complex Materials Scattering (CMS) beamline of the National Synchrotron Light Source II, a U.S. Department of Energy (DOE) Office of Science User Facility operated for the DOE Office of Science by Brookhaven National Laboratory under Contract no. DE-SC0012704. We thank Honghu Zhang for assisting in running samples at Brookhaven National Laboratory. Finally, we thank Daniel Krajovic, Ethan Rubin, Emily McGuiness, Emily Ness, Allison Wong, Taylor Larison, and Anubhav Sarmah for helpful discussions and support related to this research.

REFERENCES

- (1) Lebreton, L.; Andrady, A. Future Scenarios of Global Plastic Waste Generation and Disposal. *Palgrave Commun.* **2019**, *5* (1), 6–11.
- (2) Kaitwade, N. Plastic Market Snapshot (2023 to 2033) Future Market Insights, 2023.
- (3) Breaking the Plastic Wave: A Comprehensive Assessment of Pathways towards Stopping Ocean Plastic Pollution; the Pew Charitable Trusts, 2020.
- (4) Hopewell, J.; Dvorak, R.; Kosior, E. Plastics Recycling: Challenges and Opportunities. *Philos. Trans R Soc. Lond B Biol. Sci.* **2009**, 364 (1526), 2115–2126.
- (5) Filiciotto, L.; Rothenberg, G. Biodegradable Plastics: Standards, Policies, and Impacts. *ChemSusChem* **2021**, *14* (1), 56–72.
- (6) Schneiderman, D. K.; Hillmyer, M. A. 50th Anniversary Perspective: There Is a Great Future in Sustainable Polymers. *Macromolecules* **2017**, *50* (10), 3733–3749.
- (7) Lim, L.-T.; Auras, R.; Rubino, M. Processing Technologies for Poly(Lactic Acid). *Prog. Polym. Sci.* **2008**, 33 (8), 820–852.
- (8) Miller, S. A. Sustainable Polymers: Opportunities for the Next Decade. *ACS Macro Lett.* **2013**, *2* (6), 550–554.
- (9) Bioplastics Market Development Update 2023; European Bioplastics, 2023.
- (10) Polylactic Acid Market Analysis: Industry Market Size, Plant Capacity, Production Operating Efficiency, Technology, Demand & Supply, End-User Industries, Sales Channel, Regional Demand, Foreign Trade, Company Share, Manufacturing Process, Policy and Regulatory Landscape, 2015–2035; ChemAnalyst, 2023.

- (11) Jem, K. J.; Tan, B. The Development and Challenges of Poly (Lactic Acid) and Poly (Glycolic Acid). *Adv. Ind. Eng. Polym. Res.* **2020**, 3 (2), 60–70.
- (12) Sin, L. T.; Tueen, B. S. Polylactic Acid: A Practical Guide for the Processing, Manufacturing, and Applications of PLA; William Andrew, 2019
- (13) Taib, N.-A. A. B.; Rahman, M. R.; Huda, D.; Kuok, K. K.; Hamdan, S.; Bakri, M. K. B.; Julaihi, M. R. M. B.; Khan, A. A Review on Poly Lactic Acid (PLA) as a Biodegradable Polymer. *Polym. Bull.* **2023**, *80* (2), 1179–1213.
- (14) Struik, L. C. E. Physical Aging in Plastics and Other Glassy Materials. *Polym. Eng. Sci.* 1977, 17 (3), 165–173.
- (15) Haugan, I. N.; Lee, B.; Maher, M. J.; Zografos, A.; Schibur, H. J.; Jones, S. D.; Hillmyer, M. A.; Bates, F. S. Physical Aging of Polylactide-Based Graft Block Polymers. *Macromolecules* **2019**, 52 (22), 8878–8894.
- (16) Pan, P.; Zhu, B.; Inoue, Y. Enthalpy Relaxation and Embrittlement of Poly(l-Lactide) during Physical Aging. *Macromolecules* **2007**, 40 (26), 9664–9671.
- (17) Argon, A. S. The Physics of Deformation and Fracture of Polymers; Cambridge University Press: Cambridge, 2013; ..
- (18) Bucknall, C. B. Toughened Plastics; Springer Netherlands: Dordrecht, 1977; ...
- (19) Semba, T.; Kitagawa, K.; Ishiaku, U. S.; Hamada, H. The Effect of Crosslinking on the Mechanical Properties of Polylactic Acid/Polycaprolactone Blends. *J. Appl. Polym. Sci.* **2006**, *101* (3), 1816—1825.
- (20) Vilay, V.; Mariatti, M.; Ahmad, Z.; Pasomsouk, K.; Todo, M. Characterization of the Mechanical and Thermal Properties and Morphological Behavior of Biodegradable Poly(L-Lactide)/Poly(ε-Caprolactone) and Poly(L-Lactide)/Poly(Butylene Succinate-Co-L-Lactate) Polymeric Blends. *J. Appl. Polym. Sci.* **2009**, *114* (3), 1784–1792.
- (21) Delgado-Aguilar, M.; Puig, R.; Sazdovski, I.; Fullana-i-Palmer, P. Polylactic Acid/Polycaprolactone Blends: On the Path to Circular Economy, Substituting Single-Use Commodity Plastic Products. *Materials* **2020**, *13* (11), 2655.
- (22) Ostafinska, A.; Fortelny, I.; Nevoralova, M.; Hodan, J.; Kredatusova, J.; Slouf, M. Synergistic Effects in Mechanical Properties of PLA/PCL Blends with Optimized Composition, Processing, and Morphology. *RSC Adv.* **2015**, 5 (120), 98971–98982.
- (23) Anderson, K. S.; Hillmyer, M. A. The Influence of Block Copolymer Microstructure on the Toughness of Compatibilized Polylactide/Polyethylene Blends. *Polymer* **2004**, *45* (26), 8809–8823.
- (24) Ruiz-Silva, E.; Rodríguez-Ortega, M.; Rosales-Rivera, L. C.; Moscoso-Sánchez, F. J.; Rodrígue, D.; González-Núñez, R. Rotational Molding of Poly(Lactic Acid)/Polyethylene Blends: Effects of the Mixing Strategy on the Physical and Mechanical Properties. *Polymers* **2021**, *13* (2), 217.
- (25) Homklin, R.; Hongsriphan, N. Mechanical and Thermal Properties of PLA/PBS Co-Continuous Blends Adding Nucleating Agent. *Energy Procedia* **2013**, *34*, 871–879.
- (26) Wu, F.; Misra, M.; Mohanty, A. K. Super Toughened Poly(Lactic Acid)-Based Ternary Blends via Enhancing Interfacial Compatibility. ACS Omega 2019, 4 (1), 1955–1968.
- (27) Su, S.; Kopitzky, R.; Tolga, S.; Kabasci, S. Polylactide (PLA) and Its Blends with Poly(Butylene Succinate) (PBS): A Brief Review. *Polymers* **2019**, *11* (7), 1193.
- (28) Gu, L.; Nessim, E. E.; Li, T.; Macosko, C. W. Toughening Poly(Lactic Acid) with Poly(Ethylene Oxide)-Poly(Propylene Oxide)-Poly(Ethylene Oxide) Triblock Copolymers. *Polymer* **2018**, *156*, 261–269.
- (29) Anderson, K. S.; Schreck, K. M.; Hillmyer, M. A. Toughening Polylactide. *Polym. Rev.* **2008**, 48 (1), 85–108.
- (30) Nofar, M.; Sacligil, D.; Carreau, P. J.; Kamal, M. R.; Heuzey, M.-C. Poly (Lactic Acid) Blends: Processing, Properties and Applications. *Int. J. Biol. Macromol.* **2019**, *125*, 307–360.
- (31) McCutcheon, C. J.; Zhao, B.; Jin, K.; Bates, F. S.; Ellison, C. J. Crazing Mechanism and Physical Aging of Poly(Lactide) Toughened

- with Poly(Ethylene Oxide)-Block-Poly(Butylene Oxide) Diblock Copolymers. *Macromolecules* **2020**, 53 (22), 10163–10178.
- (32) McCutcheon, C. J.; Zhao, B.; Ellison, C. J.; Bates, F. S. Crazing and Toughness in Diblock Copolymer-Modified Semicrystalline Poly(l-Lactide). *Macromolecules* **2021**, *54* (23), 11154–11169.
- (33) Zhao, B.; McCutcheon, C. J.; Jin, K.; Lyadov, I.; Zervoudakis, A. J.; Bates, F. S.; Ellison, C. J. Enhanced Mechanical Properties of Uniaxially Stretched Polylactide/Poly(Ethylene Oxide)-b-Poly(Butylene Oxide) Blend Films. ACS Appl. Polym. Mater. 2022, 4 (11), 8705–8714.
- (34) Coote, J. P.; Zhao, B.; McCutcheon, C. J.; Larson, M. C.; Lyadov, I.; Bates, F. S.; Ellison, C. J. Biaxial Toughening in Uniaxially Stretched Films of Block Polymer-Modified Semicrystalline Poly(I-Lactide). ACS Appl. Polym. Mater. 2024, 6 (9), 5462–5472.
- (35) Li, T.; Zhang, J.; Schneiderman, D. K.; Francis, L. F.; Bates, F. S. Toughening Glassy Poly(Lactide) with Block Copolymer Micelles. *ACS Macro Lett.* **2016**, *5* (3), 359–364.
- (36) Antoine, S.; Geng, Z.; Zofchak, E. S.; Chwatko, M.; Fredrickson, G. H.; Ganesan, V.; Hawker, C. J.; Lynd, N. A.; Segalman, R. A. Non-Intuitive Trends in Flory—Huggins Interaction Parameters in Polyether-Based Polymers. *Macromolecules* **2021**, *54* (14), 6670–6677.
- (37) Kramer, E. J. Microscopic and Molecular Fundamentals of Crazing. In *Crazing in Polymers*; Kausch, H. H., Ed.; Springer: Berlin, Heidelberg, 1983; pp 1–56..
- (38) Bucknall, C. B.; Smith, R. R. Stress-Whitening in High-Impact Polystyrenes. *Polymer* **1965**, *6* (8), 437–446.
- (39) Donald, A. M.; Kramer, E. J. Craze Initiation and Growth in High-Impact Polystyrene. *J. Appl. Polym. Sci.* **1982**, 27 (10), 3729–3741
- (40) Gilbert, D. G.; Donald, A. M. Toughening Mechanisms in High Impact Polystyrene. *J. Mater. Sci.* **1986**, *21* (5), 1819–1823.
- (41) Bucknall, C. B.; Clayton, D. Rubber-Toughening of Plastics. J. Mater. Sci. 1972, 7 (2), 202–210.
- (42) Jang, B. Z.; Uhlmann, D. R.; Sande, J. B. V. The Rubber Particle Size Dependence of Crazing in Polypropylene. *Polym. Eng. Sci.* 1985, 25 (10), 643–651.
- (43) Steger, T. R.; Nielsen, L. E. Microvoid Formation during Deformation of High-Impact Polystyrene. *J. Polym. Sci., Polym. Phys. Ed.* 1978, 16 (4), 613–625.
- (44) Cho, K.; Yang, J.; Il, B.; Chan, K.; Park, E. Notch Sensitivity of Polycarbonate and Toughened Polycarbonate. *J. Appl. Polym. Sci.* **2003**, 89 (11), 3115–3121.
- (45) Kramer, E. J.; Berger, L. L. Fundamental Processes of Craze Growth and Fracture. In *Crazing in Polymers* Vol. 2; Kausch, H.-H., Ed.; Springer: Berlin, Heidelberg, 1990; pp 1–68.
- (46) Argon, A. S.; Cohen, R. E. Crazing and Toughness of Block Copolymers and Blends. In *Crazing in Polymers* Vol. 2; Kausch, H.-H., Ed.; Springer: Berlin, Heidelberg, 1990; pp 301–351..
- (47) Bucknall, C. B. New Criterion for Craze Initiation. *Polymer* **2007**, 48 (4), 1030–1041.
- (48) Bucknall, C. B.; Paul, D. R. Notched Impact Behavior of Polymer Blends: Part 1: New Model for Particle Size Dependence. *Polymer* **2009**, *50* (23), 5539–5548.
- (49) Bucknall, C. B.; Paul, D. R. Notched Impact Behaviour of Polymer Blends: Part 2: Dependence of Critical Particle Size on Rubber Particle Volume Fraction. *Polymer* **2013**, *54* (1), 320–329.
- (50) Socrate, S.; Boyce, M. C.; Lazzeri, A. A Micromechanical Model for Multiple Crazing in High Impact Polystyrene. *Mech. Mater.* **2001**, 33 (3), 155–175.
- (51) Kinloch, A. J.; Young, R. J. Fracture Behaviour of Polymers; Springer Netherlands: Dordrecht, 1995; ...
- (52) Silberberg, J.; Han, C. D. The Effect of Rubber Particle Size on the Mechanical Properties of High-Impact Polystyrene. *J. Appl. Polym. Sci.* 1978, 22 (3), 599–609.
- (53) Bai, H.; Huang, C.; Xiu, H.; Gao, Y.; Zhang, Q.; Fu, Q. Toughening of Poly(l-Lactide) with Poly(ε -Caprolactone): Combined Effects of Matrix Crystallization and Impact Modifier Particle Size. *Polymer* **2013**, *54* (19), 5257–5266.

- (54) Dağli, G.; Argon, A. S.; Cohen, R. E. Particle-Size Effect in Craze Plasticity of High-Impact Polystyrene. *Polymer* **1995**, *36* (11), 2.173–2.180.
- (55) Correa, C. A.; de Sousa, J. A. Rubber Particle Size and Cavitation Process in High Impact Polystyrene Blends. *J. Mater. Sci.* **1997**, 32 (24), 6539–6547.
- (56) Kim, K.; Arora, A.; Lewis, R. M.; Liu, M.; Li, W.; Shi, A.-C.; Dorfman, K. D.; Bates, F. S. Origins of Low-Symmetry Phases in Asymmetric Diblock Copolymer Melts. *Proc. Natl. Acad. Sci. U.S.A.* **2018**, *115* (5), 847–854.
- (57) Chang, K.; Robertson, M. L.; Hillmyer, M. A. Phase Inversion in Polylactide/Soybean Oil Blends Compatibilized by Poly(Isopreneb-Lactide) Block Copolymers. *ACS Appl. Mater. Interfaces* **2009**, *1* (10), 2390–2399.
- (58) Schmidt, S. C.; Hillmyer, M. A. Synthesis and Characterization of Model Polyisoprene–Polylactide Diblock Copolymers. *Macromolecules* **1999**, 32 (15), 4794–4801.
- (59) Frick, E. M.; Hillmyer, M. A. Synthesis and Characterization of Polylactide-Block-Polyisoprene-Block-Polylactide Triblock Copolymers: New Thermoplastic Elastomers Containing Biodegradable Segments. *Macromol. Rapid Commun.* **2000**, *21* (18), 1317–1322.
- (60) Gebizlioglu, O. S.; Beckham, H. W.; Argon, A. S.; Cohen, R. E.; Brown, H. R. A New Mechanism of Toughening Glassy Polymers. 1. Experimental Procedures. *Macromolecules* **1990**, 23 (17), 3968–3974.
- (61) Brown, H. R.; Argon, A. S.; Cohen, R. E.; Gebizlioglu, O. S.; Kramer, E. J. New Mechanism for Craze Toughening of Glassy Polymers. *Macromolecules* **1989**, 22 (2), 1002–1004.
- (62) Argon, A. S.; Cohen, R. E.; Gebizlioglu, O. S.; Brown, H. R.; Kramer, E. J. A New Mechanism of Toughening Glassy Polymers. 2. Theoretical Approach. *Macromolecules* **1990**, 23 (17), 3975–3982.
- (63) Dorgan, J. R.; Janzen, J.; Knauss, D. M.; Hait, S. B.; Limoges, B. R.; Hutchinson, M. H. Fundamental Solution and Single-Chain Properties of Polylactides. *J. Polym. Sci., Part B: Polym. Phys.* **2005**, 43 (21), 3100–3111.
- (64) González-Villa, J.; Saldívar-Guerra, E.; de León-Gómez, R. E. D.; López González, H. R.; Infante-Martínez, J. R. Kinetics of the Anionic Homopolymerizations of β–Myrcene and 4–Methylstyrene in Cyclohexane Initiated by n–Butyllithium. *J. Polym. Sci., Part A: Polym. Chem.* **2019**, *57* (21), 2157–2165.
- (65) Hillmyer, M. A.; Bates, F. S. Synthesis and Characterization of Model Polyalkane–Poly(Ethylene Oxide) Block Copolymers. *Macromolecules* **1996**, 29 (22), 6994–7002.
- (66) Fetters, L. J.; Lohse, D. J.; Richter, D.; Witten, T. A.; Zirkel, A. Connection between Polymer Molecular Weight, Density, Chain Dimensions, and Melt Viscoelastic Properties. *Macromolecules* **1994**, 27 (17), 4639–4647.
- (67) Martuscelli, E.; Silvestre, C.; Addonizio, M. L.; Amelino, L. Phase Structure and Compatibility Studies in Poly(Ethylene Oxide)/Poly(Methyl Methacrylate) Blends. *Makromol. Chem.* **1986**, *187* (6), 1557–1571.
- (68) Lee, S.; Gillard, T. M.; Bates, F. S. Fluctuations, Order, and Disorder in Short Diblock Copolymers. *AIChE J.* **2013**, *59* (9), 3502–3513
- (69) Smith, R. W.; Bryg, V. The Staining of Polymers II. *Microsc. Today* **2006**, *14* (1), 14–19.
- (70) Sinturel, C.; Bates, F. S.; Hillmyer, M. A. High χ –Low N Block Polymers: How Far Can We Go? *ACS Macro Lett.* **2015**, *4* (9), 1044–1050.
- (71) Gillard, T. M.; Phelan, D.; Leighton, C.; Bates, F. S. Determination of the Lamellae-to-Disorder Heat of Transition in a Short Diblock Copolymer by Relaxation Calorimetry. *Macromolecules* **2015**, *48* (13), 4733–4741.
- (72) Loo, Y.-L.; Register, R. A.; Ryan, A. J. Modes of Crystallization in Block Copolymer Microdomains: Breakout, Templated, and Confined. *Macromolecules* **2002**, 35 (6), 2365–2374.
- (73) Xue, F.; Chen, X.; An, L.; Funari, S. S.; Jiang, S. Soft Nanoconfinement Effects on the Crystallization Behavior of Asymmetric Poly(Ethylene Oxide)-Block-Poly(ε Caprolactone) Diblock Copolymers. *Polym. Int.* **2012**, *61* (6), 909–917.

- (74) Nakagawa, S.; Marubayashi, H.; Nojima, S. Crystallization of Polymer Chains Confined in Nanodomains. *Eur. Polym. J.* **2015**, 70, 262–275.
- (75) Floudas, G.; Vazaiou, B.; Schipper, F.; Ulrich, R.; Wiesner, U.; Iatrou, H.; Hadjichristidis, N. Poly(Ethylene Oxide-b-Isoprene) Diblock Copolymer Phase Diagram. *Macromolecules* **2001**, *34* (9), 2947–2957.
- (76) Floudas, G.; Ulrich, R.; Wiesner, U. Microphase Separation in Poly(Isoprene-b-Ethylene Oxide) Diblock Copolymer Melts. I. Phase State and Kinetics of the Order-to-Order Transitions. *J. Chem. Phys.* **1999**, *110* (1), 652–663.
- (77) Jin, H.-J.; Chin, I.-J.; Kim, M.-N.; Kim, S.-H.; Yoon, J.-S. Blending of Poly(L-Lactic Acid) with Poly(Cis-1,4-Isoprene). *Eur. Polym. J.* **2000**, 36 (1), 165–169.
- (78) Loewenhaupt, B.; Steurer, A.; Hellmann, G. P.; Gallot, Y. Microphases and Macrophases in Polymer Blends with a Diblock Copolymer. *Macromolecules* **1994**, 27 (4), 908–916.
- (79) Eom, Y.; Choi, B.; Park, S. A Study on Mechanical and Thermal Properties of PLA/PEO Blends. *J. Polym. Environ.* **2019**, 27 (2), 256–262.
- (80) Li, D.; Jiang, Y.; Lv, S.; Liu, X.; Gu, J.; Chen, Q.; Zhang, Y. Preparation of Plasticized Poly (Lactic Acid) and Its Influence on the Properties of Composite Materials. *PLoS One* **2018**, *13* (3), No. e0193520.
- (81) Alexander, L. E. X-Ray Diffraction Methods in Polymer Science; Wiley-Interscience: New York, 1969.
- (82) Van Krevelen, D. W.; Te Nijenhuis, K. Chapter 13 Mechanical Properties of Solid Polymers. In *Properties of Polymers*, 4, ed.; Van Krevelen, D. W., Te Nijenhuis, K., Eds.; Elsevier: Amsterdam, 2009; pp 383–503..
- (83) Liu, H.; Zhang, J. Research Progress in Toughening Modification of Poly(Lactic Acid). *J. Polym. Sci., Part B: Polym. Phys.* **2011**, 49 (15), 1051–1083.
- (84) Zhao, X.; Hu, H.; Wang, X.; Yu, X.; Zhou, W.; Peng, S. Super Tough Poly(Lactic Acid) Blends: A Comprehensive Review. RSC Adv. 2020, 10 (22), 13316–13368.
- (85) Argon, A. S. Role of Heterogeneities in the Crazing of Glassy Polymers. *Pure Appl. Chem.* **1975**, 43 (1–2), 247–272.
- (86) Aliotta, L.; Cinelli, P.; Coltelli, M. B.; Lazzeri, A. Rigid Filler Toughening in PLA-Calcium Carbonate Composites: Effect of Particle Surface Treatment and Matrix Plasticization. *Eur. Polym. J.* **2019**, *113*, 78–88.
- (87) Wang, D.; Wilkie, C. A. In-Situ Reactive Blending to Prepare Polystyrene—Clay and Polypropylene—Clay Nanocomposites. *Polym. Degrad. Stab.* **2003**, 80 (1), 171–182.
- (88) Gao, Y.; Liu, L.; Zhang, Z. Mechanical Performance of Nano-CaCO3 Filled Polystyrene Composites. *Acta Mechanica Solida Sinica* **2009**, 22 (6), 555–562.
- (89) Qin, J.; Argon, A. S.; Cohen, R. E. Toughening of Glassy Polymers by Prepackaged Deformation-Activated Diluents. *J. Appl. Polym. Sci.* **1999**, 71 (9), 1469–1490.
- (90) Spiegelberg, S. H.; Argon, A. S.; Cohen, R. E. Kinetics of Crazing in Polybutadiene/Polystyrene Blends. *J. Appl. Polym. Sci.* **1994**, 53 (9), 1251–1259.
- (91) Spiegelberg, S. H.; Argon, A. S.; Cohen, R. E. Measurements of Craze Velocities in Polystyrene-Polybutadiene Blends. *J. Appl. Polym. Sci.* **1993**, 48 (1), 85–97.
- (92) Brown, N.; Metzger, B. D. The Dependence of Craze Velocity on the Pressure and Temperature of the Environmental Gas. *J. Polym. Sci., Polym. Phys. Ed.* **1980**, *18* (9), 1979–1992.
- (93) Brown, N. Dependence of Craze Velocity on Stress and on the Absorption and Diffusion of Environmental Gases. *J. Macromol. Sci., Part B* **1981**, *19* (3), 387–399.
- (94) Kefalas, V. A.; Argon, A. S. The Effect of Environmental Water on the Craze Growth Rate of Atactic Polystyrene. *J. Mater. Sci.* **1988**, 23 (1), 253–258.